JOURNAL OF CATALYSIS 122, 240–246 (1990)

Effect of Surface Roughness on Particle Size Predictions from Photoemission Results

S. MARK DAVIS

Exxon Research and Development Laboratories, P.O. Box 2226, Baton Rouge, Louisiana 70821

Received March 28, 1989; revised October 20, 1989

Models are developed to illustrate the influence of surface roughness on particle size predictions derived from (dispersed phase/support phase) photoemission intensity ratios. Both low area model systems and high area practical catalysts are considered. Example applications in studies of palladium dispersed on alumina suggest that a diamond-type model combining the effects of surface roughness and a high surface area provides reasonable particle size estimates for practical catalysts. © 1990 Academic Press, Inc.

INTRODUCTION

Probably the best-known method for estimating dispersed phase particle sizes from X-ray photoemission results is based on analysis of the dispersed phase/support phase (DP/SP) XPS intensity ratio (*1–7*). Variations of this approach have considered variable particle morphologies (*1*) and the effect of a high support surface area on the particle size prediction by representing the catalyst as a flat surfaced, multilayered slab material (*2*). While idealized flat surfaces can often be realized in experimental studies of model catalysts, practical catalyst surfaces are rough on an atomic scale regardless of the method of sample preparation. It is the purpose of this communication to emphasize that surface roughness can have a significant influence on particle size estimates based on the magnitude of the (DP/SP) XPS intensity ratio.

CONCEPTS

We begin by reviewing the basic dependence of the (DP/SP) intensity ratio on the dispersed phase particle size d, for an ideal model catalyst which contains small particles dispersed on a flat surface of semi-infinite thickness. If we assume emission normal to the macroscopic surface, the (DP/SP) intensity ratio is represented by a function of the form (*1*)

$$\frac{I_m(d)}{I_s(d)} = \frac{\rho_m \sigma_m T_m \lambda_m}{\rho_s \sigma_s T_s \lambda_s} \times \left[\frac{F(L, s, d)\beta(d, \lambda_m)}{1 - F(L, s, d)\beta(d, \lambda_s)}\right], \quad (1)$$

where ρ_i is the atomic density, σ_i is the photoionization cross section (*7*), T_i is the instrumental detection efficiency, $F(L, s, d)$ is the fraction of the support surface area covered by the dispersed phase, and $\beta(d, \lambda_i)$ is an attenuation factor which is characteristic of the dispersed phase particle size and shape and the attenuation lengths λ_s and λ_m for the support and dispersed phase photoelectrons, respectively. As discussed previously (*1*), $F(L, s, d)$ is a simple function of the dispersed phase loading L, the support surface area s, and the particle size d, along with the dispersed phase bulk density D. The forms of $F(L, s, d)$ and $\beta(d, \lambda_i)$ for cubic and spherical particles are compared in Table 1 (*1*). Alternate particle shapes are considered elsewhere (*4*).

The problem of roughness and its effect on the angular distribution of XPS intensities was delineated by Fadley *et al.* (*6*) for continuous, uniform overlayers on a one-dimensional sinusoidal surface. We now extend these concepts to "broken overlayers" represented by spherical and cubic particles dispersed on idealized triangular rough surfaces as exemplified in Fig. 1. At

0021-9517/90 $3.00

TABLE 1

Surface Coverages and Attenuation Factors for Spherical and Cubic Particles

Particle shape	Cube	Sphere
Dimensions	d = edge length	d = diameter
Fractional coverage $F(L, s, d)$	L/Dsd	$3L/2Dsd$
Attenuation factor $\beta(d, \lambda)$	$1 - \exp(-d/\lambda)$	$1 - \frac{2\lambda^2}{d^2}[1 - \exp(-d/\lambda)] + \frac{2\lambda}{d}\exp(-d/\lambda)$

any point along the rough surface, the true escape angle ϕ' is defined as the angle between the escape direction and the microscopic surface tangent, and the XPS intensities for the dispersed and support phases are obtained by taking into account the angular dependence of the surface coverage $F(L, s, d)$ and attenuation factor $\beta(d, \lambda)$ as viewed from the direction of the energy analyzer. For spherical particles, the attenuation factor shows no angular dependence, although the surface coverage appears to be increased by the factor $1/\sin \phi'$ relative to the actual surface coverage $F(L, s, d) = 3L/2Dsd$. Accordingly, the ratio of the rough and flat surface (DP/SP) intensity ratios can be simply expressed by

$$\frac{(I_m/I_s)^{rough}}{(I_m/I_s)^{flat}} = \frac{1 - F(L, s, d)\beta(d, \lambda_s)}{\sin \phi' - F(L, s, d)\beta(d, \lambda_s)}. \quad (2)$$

Figure 2 displays the dependence of Eq. 2 on average particle size at two surface coverages for several values of the average take-off angle $\langle\phi'\rangle$. It is clearly seen that roughness significantly increases the magnitude of the (DP/SP) intensity ratio. Because the apparent coverage is increased, the contribution of the dispersed phase to the total XPS intensity is increased, whereas that from the support is decreased. The deviation from flat surface behavior becomes pronounced for small take-off angles, high coverages, and large particle sizes.

By considering the angular dependence of $\beta(d, \lambda)$ (*4*), it can be further shown that deviations from flat surface behavior depend strongly on the morphology of the dispersed phase particles. As an example, Fig. 3 compares the behavior for cubic, spherical, and prismatic particles on triangular surfaces with $F(L, s, d) = 0.5$ and $\phi' = 45°$. Cubic particles show the strongest devia-

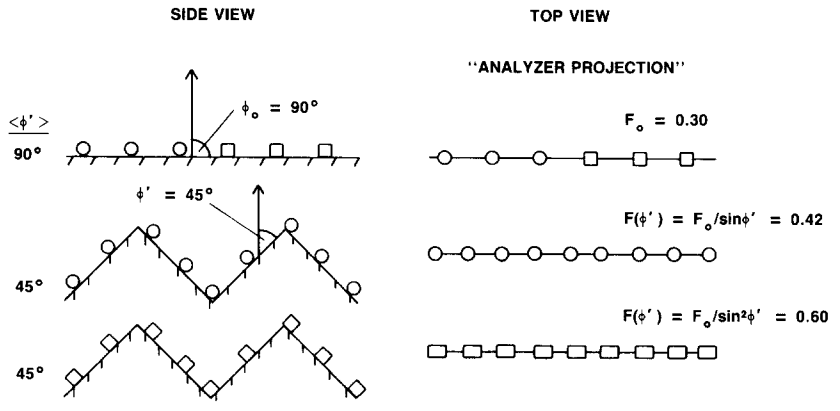

FIG. 1. Idealized models for one-dimensional rough surfaces showing triangular support surfaces partially covered by cubic or spherical dispersed phase particles. Roughness causes the average electron escape angle to deviate from 90°. Additionally, the fractional dispersed phase surface coverage as viewed from the energy analyzer appears to be increased compared to that of a flat surface.

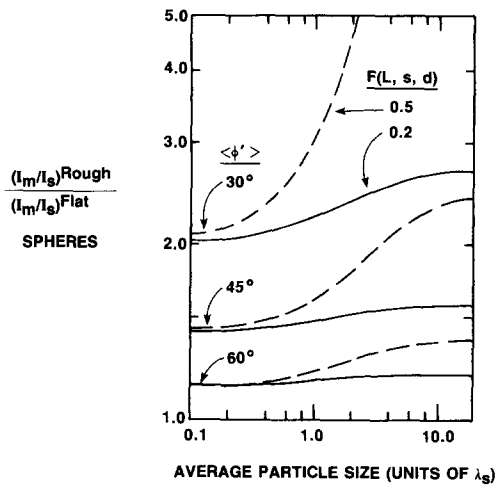

FIG. 2. The metal-to-support XPS intensity ratio for spherical particles supported on triangular rough surfaces is compared as a function of particle size with the corresponding ratio for a flat surface with $\phi = 90°$. Different curves represent rough surfaces that are distinguishable according to the dispersed phase surface coverage and average take off angle $\langle\phi'\rangle$. The deviation from flat surface behavior increases with large particles, high coverages, and small take-off angles.

tion, whereas prismatic particles show modest changes from flat surface behavior. In general, it appears that particle sizes estimated for rough, model catalyst surfaces from the (DP/SP) intensity ratio assuming a flat surface morphology will represent a *LOWER LIMIT* to the true particle size.

The effect of surface roughness on particle size estimates for practical catalysts can be explored by comparing predictions from two models that are illustrated in Fig. 4. The first is that proposed by Kerkhof and Moulijn (*2*) as an extension of the model of Defossé *et al.* (*7*) wherein the catalyst is constructed of slabs with thickness b containing dispersed phase particles distributed on both upper and lower surfaces. In our rough surface model, the support is based on a loosely packed array of diamond-shaped particles with $\langle\phi'\rangle = 45°$. In both cases, we assume random registry between layers of support material and that the DP loading is small enough that self-attenuation of the DP-intensity by dispersed phase particles in alternate layers may be neglected. With these constraints, the DP and SP intensities can be evaluated using a layer-by-layer analysis that was reported previously (*2, 4*). For the diamond model with cubic dispersed phase particles, the (DP/SP) intensity ratio for the multi-

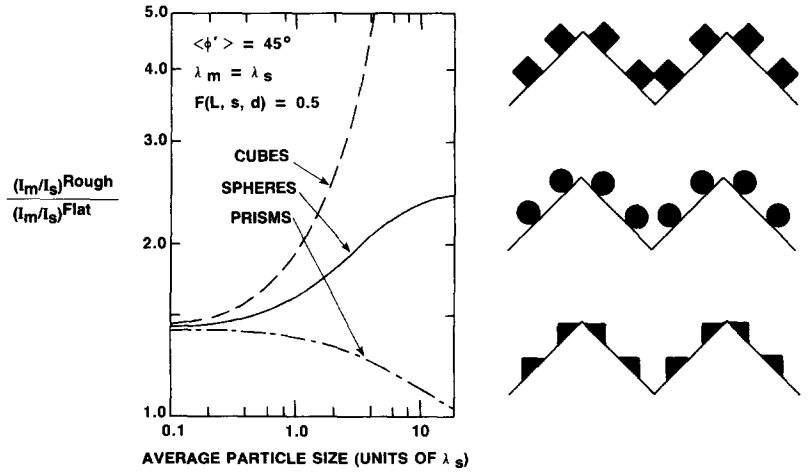

FIG. 3. The metal-to-support XPS intensity ratio for triangular rough surfaces is compared as a function of particle size with that for a flat surface. Different curves reflect variable dispersed phase particle shapes with $\langle\phi'\rangle = 45°$ and $F(D, s, d) = 0.50$ constrained constant.

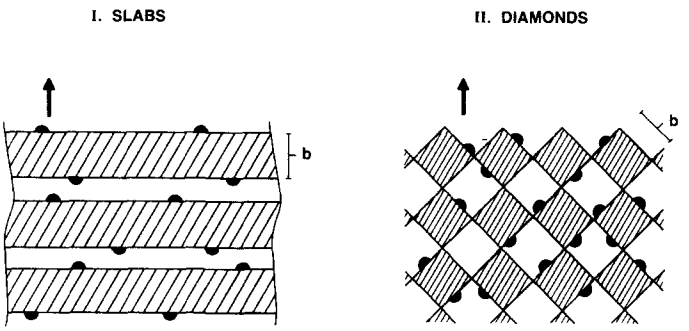

FIG. 4. Idealized slab and diamond models for high area heterogeneous catalysts. While the diamond layers are shown to be in registry, this is not a requirement of the model.

layer (ML) catalyst becomes

$$\left(\frac{I_m(d)}{I_s(d)}\right)^{ML}_{cubes} = \frac{\rho_m \sigma_m T_m \lambda_m}{\rho_s \sigma_s T_s \lambda_s} \times \frac{2\eta'_m(2 - \beta'(b, \lambda^s_m))}{\beta'(b, \lambda^s_m)[1 - 2\eta'_s(2 - \beta'(b, \lambda_s))]}, \quad (3)$$

where

$$\beta'(b, \lambda) = 1 - \frac{\lambda}{\sqrt{2}b} \times (1 - \exp(-\sqrt{2}b/\lambda)), \quad (4)$$

$\eta'_i = F(L, s, d)\beta'(d, \lambda_i)$, and λ^s_m represents the attenuation length for dispersed phase photoelectrons in the support material. Alternately, for the diamond model with spherical DP particles

$$\left(\frac{I_m(d)}{I_s(d)}\right)^{ML}_{spheres} = \frac{\rho_m \sigma_m T_m \lambda_m}{\rho_s \sigma_s T_s \lambda_s} \times \frac{\sqrt{2}\eta_m(2 - \beta'(b, \lambda^s_m))}{\beta'(b, \lambda^s_m)[1 - \sqrt{2}\eta_s(2 - \beta'(b, \lambda_s))]}, \quad (5)$$

where $\eta_i = L(D, s, d)\beta(d, \lambda_i)$ as given in Table 1. For cubic support particles, $b = 6/sD_s$, whereas for slabs, $b = 2/sD_s$, where D_s is the support phase bulk density.

APPLICATIONS

To illustrate the influence of roughness on particle size estimates from the (DP/SP) XPS intensity ratio, we consider applications in studies of a 3.3% Pd/Al_2O_3 catalyst with variable activation severity. The catalysts were investigated as pressed wafers (ca. 2 cm^2 × 0.2 mm) mounted on copper sample holders which could be transferred between a pretreatment reactor and a Leybold surface analysis chamber using magnetic manipulators. XPS data were collected using unmonochromatized Al(K_α) radiation and a hemispherical energy analyzer which was operated at 50 eV pass energy. Data acquisition and manipulation were executed using a HP1000 computer equipped with the DS5 software package. The attenuation lengths used in our particle size calculations correspond to average values based on the formulas proposed by Seah and Dench (*9*) and Tanuma *et al.* (*10*). Standard bulk phase densities were employed along with Scofield photoionization cross sections (*11*).

The 3.3% Pd/Al_2O_3 catalyst was prepared by incipient wetness impregnation of Al_2O_3 (66 m^2/g, Cyanamid γ-Al_2O_3 precalcined 1000°C) with $Pd(NH_3)_4(NO_3)_2$ followed by drying and air calcination at 250–600°C. Figure 5 shows Pd(3*d*) XPS data for unreduced catalysts; corresponding results for reduced catalysts were shown previously (*4*). Table 2 summarizes Pd(3*d*)/Al(2*s*) XPS intensity ratios measured before and after *in situ* H_2 reduction at 500°C for 2 hr. Also included are particle size estimates based on the slab and diamond models. These calculations assume cubic dispersed phase

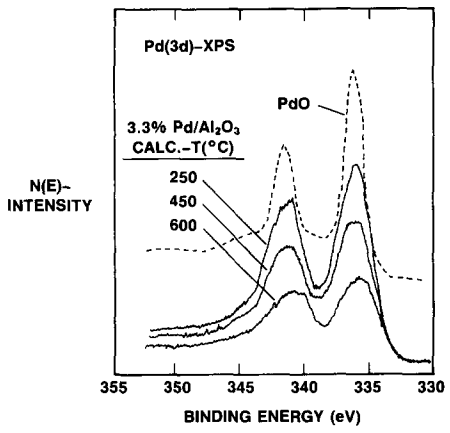

FIG. 5. Palladium (3*d*) XPS results are compared for PdO and a 3.3% Pd/Al_2O_3 catalyst precalcined at 250–600°C. Binding energies are referred to Al(2*s*) at 119.0 eV.

morphology, and, in the unreduced catalysts, it is further assumed that palladium is present as a PdO-like phase. The latter assumption is justified by 0.6 to 1.0-eV Pd($3d_{5/2}$) chemical shifts which were detected after reduction (*12*).

It is apparent from Table 2 that the Pd/Al intensity ratio decreased sharply with increasing calcination severity. These changes appear to arise from sintering of the dispersed phase during high-temperature air treatment. Hydrogen treatments were accompanied by a further moderate decrease in the magnitude of the Pd/Al XPS intensity ratio.

The particle size predictions included in Table 2 further indicate that sintering occurs during high-temperature air treatment and hydrogen reduction. It is more interesting to note that surface roughness has a strong influence on the particle size predictions. As expected from Figs. 2 and 3, roughness significantly increases the particle size estimates compared to those on a flat surface. Because of the relatively low support surface area associated with this example, contributions to the dispersed phase intensity from microporous regions below the surface have only a minor influence on the particle size predictions.

Very recently, an alternate approach for particle size estimation from XPS results was formulated on the basis of the intensity ratio for two dispersed-phase core levels with different kinetic energies (*4*). Advantages of this approach include a reduced de-

TABLE 2

Particle Size Estimates for 3.3% Pd/Al_2O_3

Precalcination conditions	Pd(3*d*)/Al(2*s*)XPS intensity ratio (±ca. 10%)	Particle size (Å) by model from Pd(3*d*)/Al(2*s*)[a]		Particle size (Å) from other methods		
		Diamond	Slab	Pd(3*d*)/Pd(MNN)[b] intensity ratio	Electron microscopy	Oxygen chemisorption
A. Unreduced catalysts						
250°C–0.5 hr	0.70	26	2	4	—	—
250°C–0.5 hr	0.49	51	20	21	30	—
600°C–20 hr	0.32	91	44	76	55	—
B. Reduced catalysts[c]						
250°C–0.5 hr	0.46	41	17	14	21	<10 (O/Pd = 1.2)
450°C–2 hr	0.33	64	31	43	44	49 (O/Pd = 0.28)
600°C–20 hr	0.21	110	56	130	74	92 (O/Pd = 0.15)

[a] Calculated using λ_{Pd} in Pd = 16.7 Å; λ_{Pd} in PdO = 22.6 Å; λ_{Pd} in Al_2O_3 = 21.9 Å; λ_{Al} in Al_2O_3 = 24.0 Å.
[b] Discussed in Ref. (*4*).
[c] After H_2 treatment at 500°C–2 hr.

pendence on surface roughness and catalyst physical properties, although a variety of elements are not accessible by this approach due to a lack of core levels with appropriate energies and/or sufficient intensity (*4*). Particle size estimates from either the (DP/SP) or (DP/DP) intensity ratio require an assumed particle morphology which can only be justified by application of other techniques. Owing to the different physical characterisitcs of these methods, it is advisable when feasible to apply both approaches, preferably in combination with alternate methods such as electron microscopy, X-ray line broadening, or chemisorption.

As an example test of self-consistency, Table 2 compares particle size estimates for 3.3% Pd/Al_2O_3 as determined by electron microscopy, static oxygen chemisorption, and photoemission methods. Particle sizes predicted from analysis of the Pd(3*d*)/Al(2*s*) intensity ratio generally bracketed those for conventional methods. Specifically, the slab model predictions were consistently smaller than those for other techniques, whereas diamond model particle sizes were systematically larger. This comparison suggests that the actual behavior for experimental catalysts with random packing of support particles is probably intermediate between the idealized slab and diamond model representations. For the smallest particles, including roughness in the calculation clearly did not improve the quality of the particle size estimate. However, with the larger particles, the influence of roughness is needed to reconcile differences between the slab model predictions and particle size estimates by microscopy or oxygen uptake. Even with the largest particles, the diamond representation overestimated the particle size to about the same extent that it was underestimated with the slab model. Relative to the other methods, the Pd(3*d*)/Pd(MNN) XPS intensity ratio provided similar, reasonable particle size estimates (*4*). Inaccuracies in the intensity measurements (estimated uncertainty ca. 10%), attenuation lengths, and/or improper assumptions regarding the particle morphology are also likely to contribute to differences in the XPS particle size predictions relative to the other methods.

By considering the angular dependence of $\beta(d, \lambda)$ (*4*), diamond-type representations can be developed for any angle $45° \leq \langle\phi'\rangle \leq 90°$. In principle, if the dispersed phase particle size is established from other methods, modeling of this type can be used to estimate the average degree of surface roughness for an experimental material. For the example considered here, a diamond representation with $\langle\phi'\rangle \approx 55°$ provides particle size predictions which compare more favorably with the estimates from microscopy and chemisorption.

In summary, models have been developed and exemplified to illustrate the influence of surface roughness on particle size estimates on the basis of the magnitude of (dispersed phase/support phase) photoemission intensity ratios. While these estimates are best considered only semiquantitative, they can be valuable in combined surface science and catalysis studies of highly dispersed compounds that are not easily characterized by other methods.

ACKNOWLEDGMENTS

The author acknowledges experimental contributions by W. S. Varnado, S. Lenhard, X. B. Cox, and E. Shannon along with the support of this research by the Exxon Research and Engineering Company.

REFERENCES

1. Fung, S. C., *J. Catal.* **58,** 454 (1979).
2. Kerkhof, F. P. J. M., and Moulijn, J. A., *J. Phys. Chem.* **83,** 1012 (1979).
3. Angevine, P. J., Vartul, J. C., and Delgass, W. N., *in* "Proceedings, 6th International Congress on Catalysis, London, 1976" (G. C. Bond, P. B. Wells, and F. C. Tompkins, Eds.), p. 611. The Chemical Society, London, 1977.
4. Davis, S. M., *J. Catal.* **117,** 432 (1989).
5. Davis, S. M., *Langmuir* **6,** in press (1990).
6. Fadley, S. C., Baird, R. J., Seikhaus, W., Novakov, T., and Bergstrom, S. A. L., *J. Electron Spectrosc. Relat. Phenom.* **4,** 93 (1974).
7. Defossé, C., Canesson, P., Rouxhet, P. G., and

Delmon, B., *J. Catal.* **51,** 269 (1978); Shalvoy, R. B., and Reucroft, P. J., *J. Electron Spectroc. Relat. Phenom.* **12,** 351 (1977).
8. Davis, S. M., and Somorjai, G. A., *Bull. Soc. Chim. Fr.* **1985,** 271 (1985).
9. Seah, M. P., and Dench, W. A., *Surf. Interface Anal.* **1,** 2 (1979).
10. Tanuma, S., Powell, C. J., and Penn, D. R., *Surf. Sci.* **192,** L849 (1987).
11. Scofield, J. H., *J. Electron Spectrosc. Relat. Phenom.* **8,** 129 (1976).
12. Wagner, C. D., Ed., "Handbook of X-ray Photoelectron Spectroscopy." Physical Electronics, Eden Park, MN 1979.